




**Variation of charge dynamics upon antiferromagnetic transitions in the Dirac semimetal EuMnBi<sub>2</sub>**

H. Nishiyama,<sup>1</sup> H. Sakai ,<sup>2</sup> K. Nakagawa,<sup>2</sup> N. Hanasaki,<sup>2</sup> S. Ishiwata,<sup>3,4</sup> H. Masuda ,<sup>5</sup> M. Ochi,<sup>2</sup> K. Kuroki,<sup>2</sup> S. Iguchi,<sup>5</sup> T. Sasaki ,<sup>5</sup> Y. Ikemoto,<sup>6</sup> T. Moriwaki,<sup>6</sup> K. Ueda,<sup>7</sup> Y. Tokura,<sup>7,8,9</sup> and J. Fujioka<sup>1</sup>

<sup>1</sup>*Institute of Materials Science, University of Tsukuba, Ibaraki 305-8573, Japan*

<sup>2</sup>*Department of Physics, Osaka University, Osaka 560-0043, Japan*

<sup>3</sup>*Division of Materials Physics, Graduate School of Engineering Science, Osaka University, Osaka 560-8531, Japan*

<sup>4</sup>*Center for Spintronics Research Network (CSRN), Graduate School of Engineering Science, Osaka University, Osaka 560-8531, Japan*

<sup>5</sup>*Institute for Materials Research, Tohoku University, Miyagi 980-8577, Japan*

<sup>6</sup>*Japan Synchrotron Radiation Research Institute, SPring-8, Hyogo 679-5198, Japan*

<sup>7</sup>*Department of Applied Physics, University of Tokyo, Tokyo 113-8656, Japan*

<sup>8</sup>*RIKEN Center for Emergent Matter Science (CEMS), Saitama 351-0198, Japan*

<sup>9</sup>*Tokyo College, University of Tokyo, Tokyo 113-8656, Japan*



(Received 1 July 2021; accepted 25 August 2021; published 7 September 2021)

We have investigated the temperature- and field-variation of electronic state for the Dirac semimetal of EuMnBi<sub>2</sub> by means of optical spectroscopy and theoretical calculation. The optical conductivity spectra show a clear Drude peak in the paramagnetic phase, which gradually diminishes in the Mn-3*d* antiferromagnetic phase with decreasing temperature. Meanwhile, the absorption peaks due to the interband transition grow at low temperatures, resulting in a pseudogap feature with an energy scale of 0.07 eV. The analysis of Drude weight shows that the Drude response is nearly governed by the Dirac electrons at low temperatures. On the contrary, both the antiferromagnetic transition and spin reorientation of Eu-4*f* moment do not significantly change the spectra except the moderate variation of Drude weight. As a comparison, we have also investigated the charge dynamics for EuZnBi<sub>2</sub>, which is an analog without the Mn-3*d* antiferromagnetic ordering. In EuZnBi<sub>2</sub>, the optical conductivity spectra do not show the pseudogap structure, but show an intense Drude peak at all temperatures. Combined with the results of *ab initio* calculation, in EuMnBi<sub>2</sub>, it is likely that the reconstruction of electronic state driven by the Mn-3*d* antiferromagnetic ordering causes the Dirac semimetallic state with tiny hole pockets, wherein electronic states other than the Dirac band are nearly gapped-out from the Fermi level.

DOI: [10.1103/PhysRevB.104.115111](https://doi.org/10.1103/PhysRevB.104.115111)

## I. INTRODUCTION

The quantum phenomena of relativistic electron (Dirac electron or Weyl electron) in solids are subjects of intensive research in the modern condensed matter physics. A remarkable feature of relativistic electron is the small transport (effective) mass, which typically manifests itself as the quantum transport such as the quantum oscillation and quantum Hall effect. For example, the quantum Hall effect remains even at room temperature for the monolayer graphene due to the exceptionally small cyclotron mass [1,2]. The large energy scale of cyclotron energy also enables us to access the various fractional quantum Hall states by tuning the electronic state in multilayered/interface structures [3–5].

More recently, it is also demonstrated that the quantum Hall effect can be induced even in bulk materials by utilizing the coupling between the Dirac electron and magnetism [13,14,17]. Among them, EuMnBi<sub>2</sub> is a prototypical material, which shows the integer quantum Hall effect in the antiferromagnetic state. This material is a member of *AMX*<sub>2</sub>-type pnictides (*A* = Eu, alkali earth ion; *M* = Mn; *X* = Bi, Sb) [6–17], wherein the crystal structure can be viewed as the stacking of the Bi-square sublattice, the Eu-sublattice and the

MnBi-sublattice along the *c* axis as illustrated in Fig. 1(a). The electronic state nearby the Fermi energy is mainly governed by the Bi-6*p* and Mn-3*d* orbitals, and the gapped Dirac band emerges nearby the Fermi energy [18,19]. The Mn-3*d* spins antiferromagnetically order at  $T_N(\text{Mn}) = 310$  K and the Eu-4*f* moments do in a manner of the up-up-down-down along the *c* axis at  $T_N(\text{Eu}) = 22$  K [20], which manifests itself as an anomaly of resistivity [see Fig. 1(c)]. Below  $T_N(\text{Eu})$ , when the magnetic field is applied along the *c* axis, the spin reorientation (spin-flop) transition of Eu-4*f* electron occurs at  $H_f = 5.3$  T and the easy axis of Eu-4*f* moment changes from the *c* axis ( $H < H_f$ ) to the *a* or *b* axis ( $H > H_f$ ) [see Fig. 1(b)] [21,22]. In particular, the quantum Hall effect is observed above 10 T in the spin-flopped phase, wherein the tilting of Eu-4*f* moment likely causes the spin-splitting of the Dirac band [13,23,24].

As opposed to EuMnBi<sub>2</sub>, the quantum Hall state has not been clearly observed in EuZnBi<sub>2</sub>, wherein the active 3*d* spin degree of freedom of Zn is absent [13]. The coupling of the electronic state with both the Mn-3*d* and Eu-4*f* spin/moment is likely crucial to realize the quasi-two-dimensional Dirac semimetallic state in EuMnBi<sub>2</sub>, but the variation of electronic state in the course of magnetic transitions has not been well

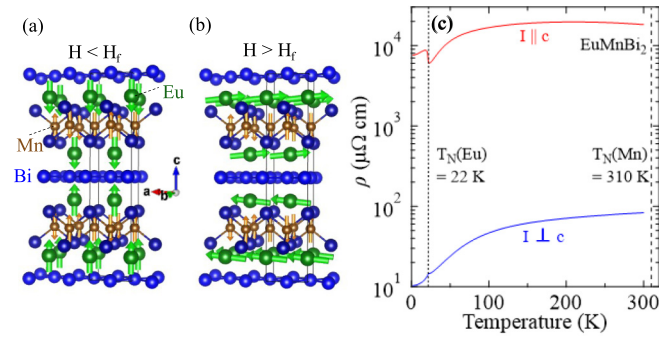


FIG. 1. The crystal and magnetic structure of  $\text{EuMnBi}_2$  (a) in the antiferromagnetic phase below  $H_f$  ( $=5.3$  T) and (b) the spin-flopped phase above  $H_f$ . The green (yellow) arrow denotes the Eu-4*f* moment (Mn-3*d* spin), respectively. The illustration is drawn by using VESTA [43]. (c) The resistivity along the *c* axis (red) and that perpendicular to the *c* axis (blue), respectively. The dashed (dotted) line denotes the antiferromagnetic transition temperature of Mn 3*d*-spin (Eu-4*f* moment), respectively. The resistivity shows a jump or kink at  $T_N(\text{Eu})$ .

understood so far. In this paper, we have investigated the electronic state for the  $\text{EuMnBi}_2$  by means of optical spectroscopy and *ab initio* calculation on the basis of density functional theory in the course of ordering of Mn-3*d* spins and Eu-4*f* moments as well as the spin-flop transition of Eu-4*f* moments under the magnetic field. Furthermore, we have also investigated the electronic state of  $\text{EuZnBi}_2$  to clarify the correlation between the electronic state and Mn-3*d* antiferromagnetic ordering.

This paper is organized as follows: First, we will present the results of optical spectra at zero magnetic field in  $\text{EuMnBi}_2$  and subsequently compare them with the results of  $\text{EuZnBi}_2$ . Then, we will show the electronic structure derived by the *ab initio* calculations for both materials. Finally, we will discuss the electronic state for  $\text{EuMnBi}_2$  under the magnetic field.

## II. EXPERIMENTAL METHODS AND THEORETICAL CALCULATION

The single crystalline samples of  $\text{EuMnBi}_2$  were grown by the self-flux method as described in Ref. [13]. The resistivity was measured by the four-probe method. For the measurements of reflectivity spectra, we have cleaved the samples and obtained a flat surface area with a typical size of 1 mm  $\times$  1 mm. The reflectivity spectra under zero magnetic field were measured in the geometry of nearly normal incidence at various temperatures from 310 K to 10 K in the energy region of 0.015–5 eV. Since the cleaved surface is usually normal to the *c* axis, the light polarization is perpendicular to the *c* axis. We used a Fourier transform spectrometer (grating-type monochromator) equipped with a microscope in the energy region of 0.015–0.7 eV (0.5–5 eV). In the region of 3–30 eV, we carried out the measurement at room temperature with use of synchrotron radiation at UV-SOR, Institute for Molecular Science (Okazaki). The optical conductivity spectrum and the loss function spectrum are derived by the Kramers-Kronig analysis. For the analysis, we adopted

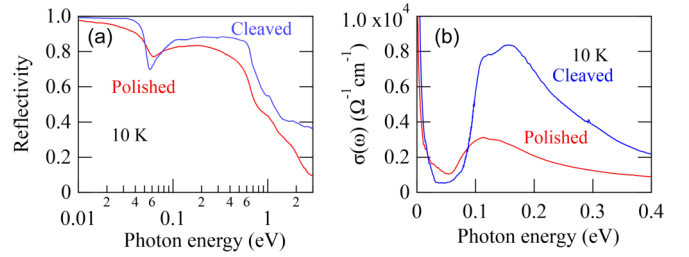


FIG. 2. (a) Reflectivity spectra and (b) optical conductivity spectra of  $\text{EuMnBi}_2$  at 10 K for the polished sample and cleaved sample.

the Hagen-Rubens-type extrapolation below 0.015 eV and  $\omega^4$ -type extrapolation above 30 eV. The reflectivity spectra under the magnetic field along the *c* axis are measured up to 14 T in the energy region of 0.025–0.1 eV at BL43IR of SPring-8. The measurements were performed in the Faraday geometry, i.e., the direction of incident/reflected light is parallel to magnetic field, and the spot size is set to be about 0.2 mm. We note that the condition of sample surface significantly affects the reflectivity spectra and optical conductivity spectra. Figures 2(a) and 2(b) show the reflectivity spectra and optical conductivity spectrum at 10 K measured for the cleaved sample and mechanically polished sample. The spectral shape is quite different with each other. It is likely that the mechanical stress or damage at surface, which is imposed during the polishing procedure, causes the deformation of the spectrum.

We performed first-principles calculation on the basis of the density functional theory with the Perdew-Burke-Ernzerhof parametrization of the generalized gradient approximation (PBE-GGA) [25] and the projector augmented wave (PAW) method [26] as implemented in the Vienna *ab initio* simulation package [27–30]. We applied the open-core treatment for the Eu-4*f* orbitals, to say, the Eu-4*f* orbitals were not explicitly treated as valence electrons for simplicity. The spin-orbit coupling was included. The G-type antiferromagnetic order of Mn atoms as observed in experiment was assumed. For  $\text{EuMnBi}_2$ , lattice parameters and atomic coordinates were taken from experiment [20]. For  $\text{EuZnBi}_2$ , we used the experimental lattice parameters [13] and optimized the atomic coordinates by calculation. The structural optimization was performed until the Hellmann–Feynman force becomes less than 0.01 eV/Å along every direction. The plane-wave cutoff energies of 350 and 380 eV were used for  $\text{EuMnBi}_2$  and  $\text{EuZnBi}_2$ , respectively. For the band-structure calculation and the structural optimization,  $16 \times 16 \times 16$  and  $10 \times 10 \times 10$  *k* meshes were used for  $\text{EuMnBi}_2$  and  $\text{EuZnBi}_2$ , respectively. For both compounds, a  $20 \times 20 \times 20$  *k* mesh was used for calculating the partial density of states.

## III. RESULTS AND DISCUSSION

Figure 3(a) shows the temperature dependence of reflectivity spectra for  $\text{EuMnBi}_2$ . The reflectivity spectra show high reflectance band below 0.6 eV at 310 K. With decreasing temperature, a dip structure, which seemingly originates from the plasma resonance due to the Drude response, gradually evolves around 0.06 eV. Figure 3(b) shows the optical

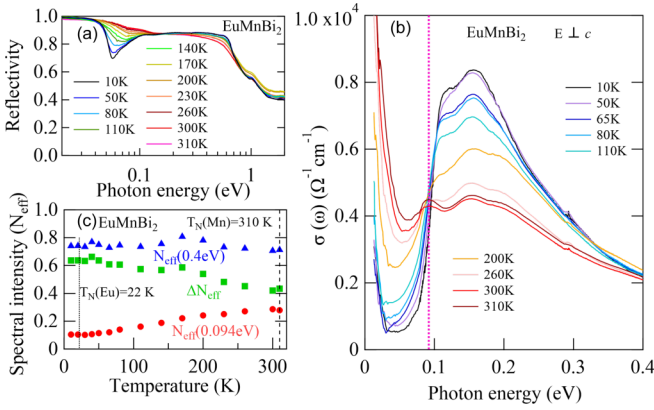


FIG. 3. (a) The reflectivity and (b) optical conductivity  $\sigma(\omega)$  spectra for  $\text{EuMnBi}_2$  measured with the light polarization perpendicular to the  $c$  axis. The vertical dotted line denotes the energy of isosbestic point (0.094 eV). (c) The spectral intensity below the cut-off energy  $\omega_c = 0.094$  eV (circle) and 0.4 eV (triangle) and their difference  $\Delta N_{\text{eff}}$ . The dotted (dashed) line denotes the antiferromagnetic transition temperature of Eu- $4f$  moment (Mn- $3d$  spin), respectively.

conductivity spectra at various temperatures. At 310 K, a spectacular Drude peak is observed below 0.05 eV. Moreover, two absorption peaks are observed around 0.1 eV and 0.15 eV, respectively. With decreasing temperature, the Drude peak gradually shrinks, and alternatively the two peaks grow, resulting in the pseudogap feature with an energy scale of 0.07 eV at 10 K. A small Drude peak as well as the pseudogap feature suggest the emergence of electronic state with tiny electron/hole pocket(s) at low temperatures.

To roughly estimate the spectral weight of Drude response (Drude weight) and absorption peaks, we calculated the effective number of electrons defined by

$$N_{\text{eff}}(\omega_c) = \frac{2m_0}{\pi e^2 N} \int_0^{\omega_c} \sigma(\omega) d\omega \quad (1)$$

Here,  $\omega_c$ ,  $m_0$ , and  $N$  are the cut-off energy, free electron mass, and number of unit formula per unit volume, respectively. Figure 3(c) shows the temperature dependence of  $N_{\text{eff}}(\omega_c)$  with  $\omega_c = 0.094$  eV and 0.4 eV and the difference between them  $\Delta N_{\text{eff}} [= N_{\text{eff}}(0.4 \text{ eV}) - N_{\text{eff}}(0.094 \text{ eV})]$ . Here, we define the energy of isosbestic point as 0.094 eV, and assume that  $N_{\text{eff}}(0.094 \text{ eV})$  represents the spectral weight in the low energy region below the pseudogap, which roughly corresponds to the Drude weight. On the other hand,  $\Delta N_{\text{eff}}$  roughly represents the spectral intensity of two absorption peaks around 0.1–0.2 eV.  $N_{\text{eff}}(0.094 \text{ eV})$  monotonically decreases with decreasing temperature and is nearly temperature independent below 50 K. On the contrary,  $\Delta N_{\text{eff}}$  is enhanced at lower temperatures and is nearly constant below 50 K. Both  $N_{\text{eff}}(0.094 \text{ eV})$  and  $\Delta N_{\text{eff}}$  appear to substantially change below  $T_N(\text{Mn})$ , but do not show remarkable change at  $T_N(\text{Eu})$ . We note that  $N_{\text{eff}}(0.4 \text{ eV})$ , which is sum of the Drude response and absorption peaks, is nearly constant over a whole temperature region. These results imply that the spectral weight of Drude response is partially transferred to that of absorption peaks with decreasing temperature below  $T_N(\text{Mn})$ . The

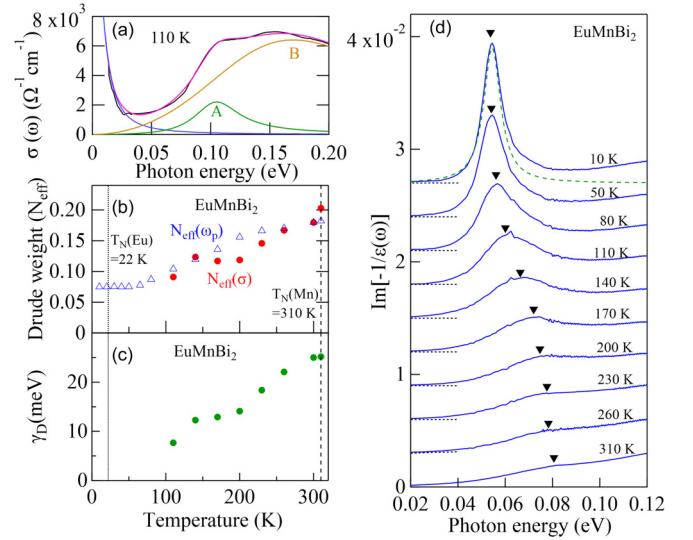


FIG. 4. (a) The fitting of optical conductivity spectra by the Drude-Lorentz model. The blue curve denotes the Drude response, and the green and yellow curves correspond to the absorption peak A and B, respectively. (b) The temperature dependence of Drude weight estimated from the Drude peak  $N_{\text{eff}}(\sigma)$  (circle) and plasma frequency  $N_{\text{eff}}(\omega_p)$  (triangle). (c) The temperature dependence of width of Drude peak  $\gamma_D$ . (d) The loss function spectra  $\text{Im}[-1/\epsilon(\omega)]$ . Each spectrum is offset for clarity. The triangle denotes the peak of plasmon resonance. The dashed line is the fitting curve of plasmon resonance at 10 K (see also the Appendix).

thermally-induced spectral change with a similar energy scale is also observed in other member of  $\text{AMnBi}_2$  with  $A = \text{Sr}, \text{Ca},$  and  $\text{Yb}$  [31–33].

To more quantitatively estimate the Drude weight, we fitted the spectra with using the following formula

$$\sigma(\omega) = \frac{\sigma_D \gamma_D^2}{\omega^2 + \gamma_D^2} + \sum_{i=A,B} \frac{S_i \gamma_i \omega_i^2 \omega^2}{(\omega^2 - \omega_i^2)^2 + \gamma_i^2 \omega^2} \quad (2)$$

The first term represents the Drude response with the dc conductivity ( $\sigma_D$ ) and peak width ( $\gamma_D$ ), respectively. The second term represents the two absorption peaks with the oscillator strength ( $S_i$ ), damping constant ( $\gamma_i$ ) and peak energy ( $\omega_i$ ), respectively. The result of fitting at 110 K is exemplified in Fig. 4(a).

Figures 4(b) and 4(c) show the  $N_{\text{eff}}$  of Drude response (the Drude weight) and peak width derived by the fitting. Both the Drude weight and peak width monotonically decrease with decreasing temperature. In particular, the peak width becomes less than 10 meV below 110 K and, thus the fitting of narrow Drude peak cannot be accurately performed. To quantify the Drude weight below 100 K, we utilized the relation between the Drude weight and plasma frequency  $\omega_p$ ; the Drude weight is scaled to  $\omega_p^2/8$  [34]. In general, the plasma resonance emerges as a peak of the imaginary part of loss function spectra  $\text{Im}[-1/\epsilon(\omega)]$ , and the peak energy corresponds to the renormalized plasma frequency  $\omega_p^* (= \omega_p/\sqrt{\epsilon_\infty})$  with  $\epsilon_\infty$  being the dielectric constant arising from the higher energy optical excitation, e.g., the interband transition. As shown in Fig. 4(d), the  $\text{Im}[-1/\epsilon(\omega)]$  spectrum shows a peak around 0.055 eV at 10 K. With increasing temperature, the peak

moves to higher energy region and gradually diminishes. We fitted the  $\text{Im}[-1/\epsilon(\omega)]$  spectrum in the scheme of Lorentz oscillator model and derived  $\omega_p^*$  (see the Appendix). The Drude weight calculated from the plasma resonance [ $N_{\text{eff}}(\omega_p)$ ] is appended in Fig. 4(b). For the calculation, we assumed  $\epsilon_\infty = 600$  so that  $N_{\text{eff}}(\omega_p)$  is consistent with the result derived by the fitting of optical conductivity [ $N_{\text{eff}}(\sigma)$ ] above 110 K. We note that the assumption of  $\epsilon_\infty = 600$  is not inconsistent with the value expected from the real part of dielectric spectra (data not shown). The Drude weight shows a sizable temperature dependence above 50 K, but is nearly temperature independent below 50 K, which is consistent with the behavior of  $N_{\text{eff}}(0.094 \text{ eV})$  shown in Fig. 3(c). With assuming the carrier density estimated by the transport measurements [13], the effective mass of electron ( $m^*$ ) is estimated to be  $0.068 m_0$  at 10 K. This value is comparable to the cyclotron mass of Dirac electrons derived by the transport measurements ( $m_c = 0.097 m_0$ ) [23], suggesting that the Drude response, or equivalently, the charge transport, is nearly governed by the Dirac electron at low temperatures. Indeed, the optical conductivity at 10 K is relatively flat in the region of 0.04–0.06 eV, which is consistent with the expected behavior of the interband transition due to the quasi-two-dimensional Dirac band.

Such a spectral variation on an energy scale of 0.4 eV reminds us of the charge dynamics in correlated electron materials showing the magnetic ordering or metal-insulator transition [35,36]. For example, in  $\text{BaFe}_2\text{As}_2$ , the charge dynamics changes in an energy scale of 0.3 eV in the course of Fe-3*d* antiferromagnetic ordering, resulting in the pseudogap opening and the narrow Drude peak [37–40]. In the present case, the electron correlation, or equivalently, the antiferromagnetic ordering of Mn-3*d* spins is expected to be responsible for the variation of electronic state. To clarify this possibility, we also investigated the charge transport/dynamics for  $\text{EuZnBi}_2$ , wherein the nominally divalent Zn-ion does not possess the active 3*d*-spin degree of freedom. Figure 5(a) shows the resistivity along the *c* axis and that perpendicular to the *c* axis. The former is only a few times larger than the latter in all temperatures. The anisotropy of resistivity is much smaller than the case of  $\text{EuMnBi}_2$ , wherein the *c* axis resistivity is three-orders of magnitude larger than that perpendicular to the *c* axis [see Fig. 1(c)]. Furthermore, the field dependence of magnetoresistivity does not show a clear anomaly reminiscent of the spin-flop transition unlike the case of  $\text{EuMnBi}_2$  (data not shown).

Figure 5(b) shows the reflectivity spectra of  $\text{EuZnBi}_2$  at various temperatures. The reflectivity spectra show the high reflectance band due to the Drude response below 0.5 eV at all temperatures. The optical conductivity spectra at various temperatures are shown in Fig. 5(c). The broad and intense Drude response is commonly observed at all temperatures. Consequently,  $N_{\text{eff}}(0.094 \text{ eV})$ , which is a measure of Drude weight, is nearly temperature independent as  $N_{\text{eff}}(0.4 \text{ eV})$  is [see Fig. 5(d)]. It should be noted here that the value of  $N_{\text{eff}}(0.094 \text{ eV})$  is about four times larger than that for  $\text{EuMnBi}_2$  at 10 K. These results suggest that the presence of Mn-3*d* state is an essential ingredient to cause the absorption peaks with a pseudogap feature as well as a tiny Drude response for  $\text{EuMnBi}_2$ .

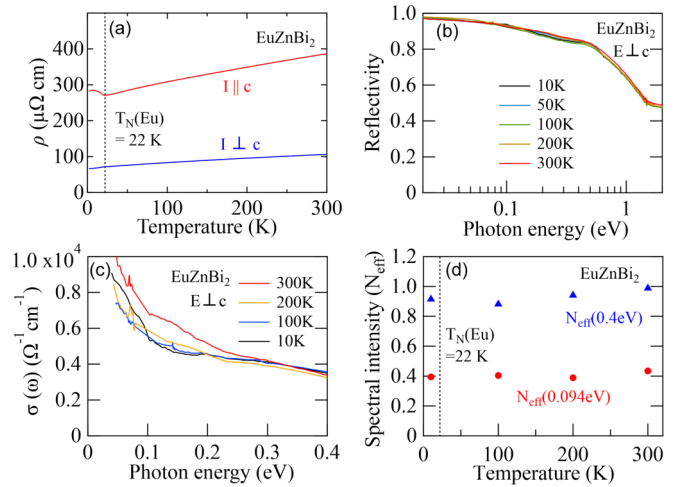


FIG. 5. (a) Temperature dependence of resistivity along the *c* axis and that perpendicular to the *c* axis. (b) The reflectivity spectra and (c) optical conductivity spectra at various temperatures. (d) The spectral intensity below the cut-off energy  $\omega_c = 0.094 \text{ eV}$  (circle) and 0.4 eV (triangle). The dotted line denotes the antiferromagnetic transition temperature of Eu-4*f* moment.

To get insight into the Mn-3*d*-state nearby the Fermi energy, we performed the *ab initio* calculation on the basis of density functional theory. Figure 6(a) shows the band structure in the ground state with the antiferromagnetic ordering of Mn-3*d* spins. Valence electrons originate from the gapped Dirac band on the  $\Gamma - X$  line, whereas many other bands lie above 0.1 eV or below  $-0.1 \text{ eV}$ . Consequently, the density of state (DOS) shows a sharp dip nearby the Fermi energy as shown in Fig. 6(b). This is in accord with the observation of small Drude response at low temperatures. The partial-DOS shows that the conduction band is mainly composed of Bi-6*p*

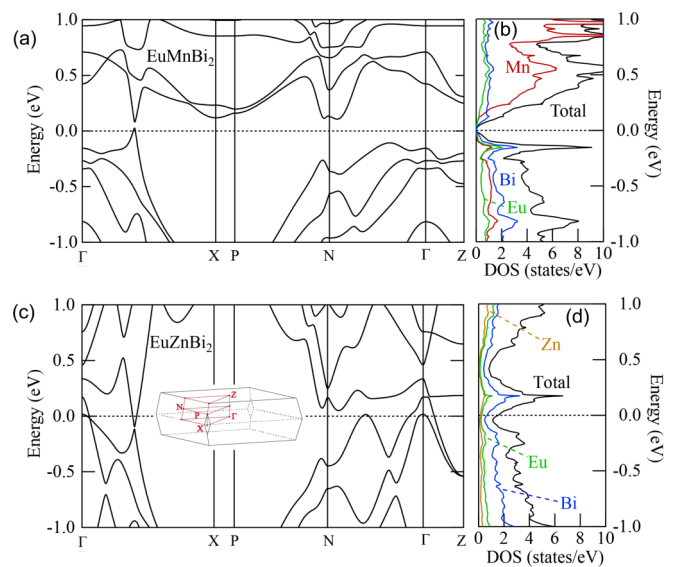


FIG. 6. First-principles band structure for (a)  $\text{EuMnBi}_2$  and (c)  $\text{EuZnBi}_2$ . (Partial) density of states for  $\text{EuMnBi}_2$  and  $\text{EuZnBi}_2$  are shown in panels (b) and (d), respectively. The inset to (c) shows the illustration of the Brillouin zone and *k* path.

state in the energy region from 0 eV ( $E_F$ ) to 0.16 eV, but is rather governed by the Mn-3d state above 0.16 eV. On the contrary, the Bi-6p state remains to be the major component of valence band down to  $-1.0$  eV. Considering that the clear absorption peaks (pseudogap feature) are absent in the energy scale below 0.4 eV in EuZnBi<sub>2</sub>, it is reasonable to assign the absorption peak to the interband transition between the occupied Bi-6p state and unoccupied Mn-3d one; although the calculated partial-DOS of the Mn-3d state has large weight around 0.5 eV, the Mn-3d state may be actually located more closely to  $E_F$  due to the correlation-induced renormalization, leading to the absorption peaks of optical conductivity around 0.1–0.2 eV. In this context, the thermally-induced blurring of absorption peak (pseudogap) and enhancement of Drude weight suggest that the electronic structure due to Mn-3d state is significantly reconstructed in the course of melting of Mn-3d antiferromagnetic order, resulting in the crossover from the Dirac semimetallic state with tiny hole pockets to the metal with incoherent charge dynamics. Although the theoretical modeling taking into account the finite temperature effect is beyond the scope of present paper, we speculate that the partial gap opening due to the electron correlation inherent to the Mn-3d state is responsible for the thermally-induced variation of electronic state.

On the other hand, in EuZnBi<sub>2</sub>, several bands cross the Fermi energy besides the Dirac band on the  $\Gamma - X$  line as shown in Figs. 6(c) and 6(d). In particular, some of them show the sizable energy dispersion along the  $c$  axis, e.g., along the  $\Gamma - Z$  line. These features are consistent with the large spectral intensity of optical conductivity spectra in the low energy region and less anisotropic transport property in EuZnBi<sub>2</sub>. In other words, these results support the scenario that the Mn-3d antiferromagnetic ordering is essential to realize the highly two-dimensional state with tiny hole pockets at low temperatures in EuMnBi<sub>2</sub>.

Having established these results, we discuss the variation of electronic state in the course of spin-flop transition of Eu-4f moment in terms of field dependence of Drude response. Since the optical conductivity- or loss function-spectra cannot be derived by means of the Kramers-Kronig analysis due to the limited energy window of measurements under the magnetic field, we evaluate the energy of plasma resonance from the the dip of reflectivity spectra. As shown in Figs. 7(a) and 7(b), the dip energy of reflectivity spectrum nearly coincides with the peak energy of loss function spectra at 0 T. With increasing the magnetic field from 0 T, the dip gradually moves to higher energies, but discontinuously shifts toward lower energies at  $H_f$ . It is known that the resonance energy under the magnetic field ( $\omega_r$ ) is described as  $\omega_r^2 = \omega_p^{*2} + \omega_c^2$  with being  $\omega_c$  the cyclotron energy [41,42]. Given that the band dispersion does not change by applying the magnetic field (the rigid band model), the field variation of  $\omega_r$  is solely attributed to  $\omega_c (= eB/m_c)$  with  $m_c$  being the cyclotron mass. In Fig. 7(c), we plot the square of resonance energy  $\omega_r^2$  as a function of magnetic field. Below  $H_f$ ,  $\omega_r^2$  increases as expected from the rigid band model. By fitting the field dependence of  $\omega_r^2$  with the function of  $\omega_p^{*2} + (eB/m_c)^2$ ,  $m_c$  is estimated to be  $0.074m_0$ . This value is nearly identical to the effective mass estimated from the Drude response at 0 T ( $=0.068m_0$ ), supporting the rigid band model below  $H_f$ . On

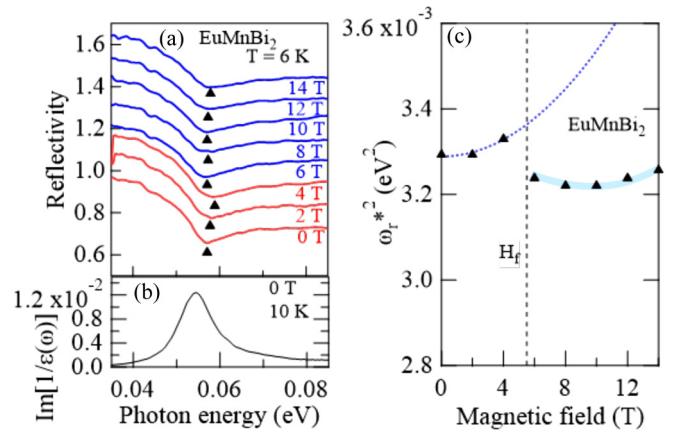


FIG. 7. (a) The reflectivity spectra measured at various magnetic fields along the  $c$  axis and at 6 K. The triangle denotes the dip structure due to the plasma resonance. (b) The loss function spectra at 10 K under zero magnetic field. (c) The square of resonance energy ( $\omega_r^2$ ) as a function of magnetic field. The vertical-dashed line represents the spin-flop transition of Eu-4f moment ( $H_f$ ). The dotted curve (hatched curve) denote the fitting results with the formula  $\omega_r^2 = \omega_p^{*2} + \omega_c^2$  (the guide to eyes).

the other hand, the field dependence of  $\omega_r^2$  above  $H_f$  cannot be simply understood from the rigid band model;  $\omega_r^2$  once decreases up to 10 T, but increases above 10 T. The previous study argues that the Dirac band shows the spin splitting and substantially deforms above  $H_f$  as the Eu-4f moment is gradually tilted toward the  $c$  axis by magnetic field [23,24]. The nonmonotonic field dependence of  $\omega_r$  may be attributed to the deformation or spin splitting of Dirac band coupled to the tilting of Eu-4f moment, whereas the specific mechanism is not simple. Regardless of the reason, considering that the field variation of  $\omega_r$  is at most 3 meV below 14 T, the energy scale of band deformation due to the spin-flop transition or tilting of Eu-4f moment is likely much smaller than that due to the Mn-3d antiferromagnetic ordering.

#### IV. CONCLUSION

In conclusion, we have investigated the temperature- and field-variation of electronic state of magnetic Dirac semimetal of EuMnBi<sub>2</sub> by means of optical spectroscopy and *ab initio* calculation. The optical conductivity spectra show a sizable temperature variation on an energy scale of 0.4 eV below the transition temperature of Mn-3d antiferromagnetic ordering [ $T_N(\text{Mn}) = 310$  K], while the spectral variation at the Eu-4f moment ordering [ $T_N(\text{Eu}) = 22$  K] is not remarkable. In particular, with decreasing temperature, the Drude peak gradually diminishes and two absorption peaks evolve around 0.1–0.2 eV, resulting in the pseudogap feature with an energy scale of 0.07 eV at 10 K. As a comparison, we investigated the optical conductivity spectra of EuZnBi<sub>2</sub>, wherein the nominally divalent Zn-ion does not possess the active 3d-spin degree of freedom. In EuZnBi<sub>2</sub>, a Drude peak with large spectral intensity remains in all temperatures, and the pseudogap feature cannot be observed even at low temperature. Combined with the results of *ab initio* calculation, it is likely that the evolution of Mn-3d antiferromagnetic ordering

significantly modifies the electronic state nearby the Fermi energy, resulting in the crossover from the incoherent metallic state at high temperature into the massive Dirac semimetallic state with tiny hole pockets at low temperatures in EuMnBi<sub>2</sub>. Finally, we also explored the plasma resonance under the magnetic field at 6 K to probe the field dependence of Drude response. The resonance energy changes only at most 3 meV at the field-induced spin-flop transition of Eu-4*f* moment (=5.3 T), suggesting that the reorientation of Eu-4*f* moment causes minimal variation of electronic state in contrast with the case of Mn-3*d*-antiferromagnetic ordering.

#### ACKNOWLEDGMENTS

We thank R. Yamada and R. Kaneko for the technical support of magneto-optical experiment. The reflectivity measurements under the magnetic field were performed at BL43IR in SPring-8 under the approval of JASRI (Proposals No. 2018B1279, No. 2019B1219, and No. 2019B1158). This

work was partly supported by Grant-In-Aid for Science Research (Nos. 16H00981, 18H01171, 18H04214, 16H06345, 19H01851) from the MEXT, by Asahi Glass Foundation and by PRESTO (No. JPMJPR15R5) and CREST (No. JPMJCR16F1), JST, Japan.

#### APPENDIX: MODEL OF LOSS FUNCTION

According to the Lorentz oscillator model, the dielectric function is written as

$$\epsilon(\omega) = \epsilon_{\infty} \left( 1 + \frac{\Omega^2}{\omega_0^2 - \omega^2 - i\omega\gamma} \right). \quad (\text{A1})$$

The loss function is written as

$$\text{Im} \left[ -\frac{1}{\epsilon(\omega)} \right] = \frac{1}{\epsilon_{\infty}} \cdot \frac{\omega\gamma\Omega^2}{(\omega_L^2 - \omega^2)^2 + \omega^2\gamma^2} \quad (\text{A2})$$

Here  $\omega_L$  is defined as  $\omega_L^2 = \omega_0^2 + \Omega^2$ .

- 
- [1] Y. Zhang, Y.-W. Tan, H. L. Stormer, and P. Kim, *Nature (London)* **438**, 201 (2005).
- [2] K. S. Novoselov, Z. Jiang, Y. Zhang, S. V. Morozov, H. L. Stormer, U. Zeitler, J. C. Maan, G. S. Boebinger, P. Kim, and A. K. Geim, *Science* **315**, 1379 (2007).
- [3] C. R. Dean, A. F. Young, P. Cadden-Zimansky, L. Wang, H. Ren, K. Watanabe, T. Taniguchi, P. Kim, J. Hone, and K. L. Shepard, *Nat. Phys.* **7**, 693 (2011).
- [4] D.-K. Ki, V. I. Fal'ko, D. A. Abanin, and A. F. Morpurgo, *Nano Lett.* **14**, 2135 (2014).
- [5] E. M. Spanton, A. A. Zibrov, H. Zhou, T. Taniguchi, K. Watanabe, M. P. Zaletel, and A. F. Young, *Science* **360**, 62 (2018).
- [6] J. Park, G. Lee, F. Wolff-Fabris, Y. Y. Koh, M. J. Eom, Y. K. Kim, M. A. Farhan, Y. J. Jo, C. Kim, J. H. Shim, and J. S. Kim, *Phys. Rev. Lett.* **107**, 126402 (2011).
- [7] J. K. Wang, L. L. Zhao, Q. Yin, G. Kotliar, M. S. Kim, M. C. Aronson, and E. Morosan, *Phys. Rev. B* **84**, 064428 (2011).
- [8] K. Wang, D. Graf, L. Wang, H. Lei, S. W. Tozer, and C. Petrovic, *Phys. Rev. B* **85**, 041101(R) (2012).
- [9] G. Lee, M. A. Farhan, J. S. Kim, and J. H. Shim, *Phys. Rev. B* **87**, 245104 (2013).
- [10] Y. Feng, Z. Wang, C. Chen, Y. Shi, Z. Xie, H. Yi, A. Liang, S. He, J. He, Y. Peng, X. Liu *et al.*, *Sci. Rep.* **4**, 5385 (2014).
- [11] J. Liu, J. Hu, H. Cao, Y. Zhu, A. Chuang, D. Graf, D. J. Adams, S. M. A. Radmanesh, L. Spinu, I. Chiorescu, and Z. Mao, *Sci. Rep.* **6**, 30525 (2016).
- [12] A. Zhang, C. Liu, C. Yi, G. Zhao, T.-L. Xia, J. Ji, Y. Shi, R. Yu, X. Wang, C. Chen, and Q. Zhang, *Nat. Commun.* **7**, 13833 (2016).
- [13] H. Masuda, H. Sakai, M. Tokunaga, Y. Yamasaki, A. Miyake, J. Shiogai, S. Nakamura, S. Awaji, A. Tsukazaki, H. Nakao, Y. Murakami, T.-H. Arima, Y. Tokura, and S. Ishiwata, *Sci. Adv.* **2**, e1501117 (2016).
- [14] J. Y. Liu, J. Yu, J. L. Ning, H. M. Yi, L. Miao, L. J. Min, Y. F. Zhao, W. Ning, K. A. Lopez, Y. L. Zhu *et al.*, *Nat. Commun.* **12**, 4062 (2021).
- [15] C. Yi, S. Yang, M. Yang, L. Wang, Y. Matsushita, S. Miao, Y. Jiao, J. Cheng, Y. Li, K. Yamaura, Y. Shi, and J. Luo, *Phys. Rev. B* **96**, 205103 (2017).
- [16] S. L. Huang, J. Kim, W. A. Shelton, E. W. Plummer, and R. Y. Jin, *Proc. Natl. Acad. Sci. USA* **114**, 6256 (2017).
- [17] H. Sakai, H. Fujimura, S. Sakuragi, M. Ochi, R. Kurihara, A. Miyake, M. Tokunaga, T. Kojima, D. Hashizume, T. Muro, K. Kuroda, T. Kondo, T. Kida, M. Hagiwara, K. Kuroki, M. Kondo, K. Tsuruda, H. Murakawa, and N. Hanasaki, *Phys. Rev. B* **101**, 081104(R) (2020).
- [18] S. V. Borisenko, D. Evtushinsky, Q. Gibson, A. Yaresko, T. Kim, M. N. Ali, B. Buechner, M. Hoesch, and R. J. Cava, *Nat. Commun.* **10**, 3424 (2019).
- [19] M. Chinotti, A. Pal, W. J. Ren, C. Petrovic, and L. Degiorgi, *Phys. Rev. B* **94**, 245101 (2016).
- [20] A. F. May, M. A. McGuire, and B. C. Sales, *Phys. Rev. B* **90**, 075109 (2014).
- [21] H. Masuda, H. Sakai, H. Takahashi, Y. Yamasaki, A. Nakao, T. Moyoshi, H. Nakao, Y. Murakami, T. Arima, and S. Ishiwata, *Phys. Rev. B* **101**, 174411 (2020).
- [22] F. Zhu, X. Wang, M. Meven, J. Song, T. Mueller, C. Yi, W. Ji, Y. Shi, J. Ma, K. Schmalzl, W. F. Schmidt, Y. Su, and T. Brückel, *Phys. Rev. Res.* **2**, 043100 (2020).
- [23] H. Masuda, H. Sakai, M. Tokunaga, M. Ochi, H. Takahashi, K. Akiba, A. Miyake, K. Kuroki, Y. Tokura, and S. Ishiwata, *Phys. Rev. B* **98**, 161108(R) (2018).
- [24] K. Tsuruda, K. Nakagawa, M. Ochi, K. Kuroki, M. Tokunaga, H. Murakawa, N. Hanasaki, and H. Sakai, *Adv. Funct. Mater.* **31**, 2102275 (2021).
- [25] J. P. Perdew, K. Burke, and M. Ernzerhof, *Phys. Rev. Lett.* **77**, 3865 (1996).
- [26] G. Kresse and D. Joubert, *Phys. Rev. B* **59**, 1758 (1999).
- [27] G. Kresse and J. Hafner, *Phys. Rev. B* **47**, 558(R) (1993).
- [28] G. Kresse and J. Hafner, *Phys. Rev. B* **49**, 14251 (1994).
- [29] G. Kresse and J. Furthmüller, *Comput. Mater. Sci.* **6**, 15 (1996).
- [30] G. Kresse and J. Furthmüller, *Phys. Rev. B* **54**, 11169 (1996).
- [31] H. J. Park, B. C. Park, M.-C. Lee, D. W. Jeong, J. Park, J. S. Kim, H. S. Ji, J. H. Shim, K. W. Kim, S. J. Moon, H.-D. Kim, D.-Y. Cho, and T. W. Noh, *Phys. Rev. B* **96**, 155139 (2017).

- [32] M. Corasaniti, R. Yang, A. Pal, M. Chinotti, L. Degiorgi, A. Wang, and C. Petrovic, *Phys. Rev. B* **100**, 041107(R) (2019).
- [33] D. Chaudhuri, B. Cheng, A. Yaresko, Q. D. Gibson, R. J. Cava, and N. P. Armitage, *Phys. Rev. B* **96**, 075151 (2017).
- [34] M. Dressel and G. Gruner, *Electrodynamics of Solids* (Cambridge University Press, Cambridge, 2001).
- [35] M. Imada, A. Fujimori, and Y. Tokura, *Rev. Mod. Phys.* **70**, 1039 (1998).
- [36] M. M. Qazilbash, J. J. Hamlin, R. E. Baumbach, L. Zhang, D. J. Singh, M. B. Maple, and D. N. Basov, *Nat. Phys.* **5**, 647 (2009).
- [37] M. Nakajima, T. Liang, S. Ishida, Y. Tomioka, K. Kihou, C. H. Lee, A. Iyo, H. Eisaki, T. Kakeshita, T. Ito, and S. Uchida, *Proc. Natl. Acad. Sci. USA* **108**, 12238 (2011).
- [38] S. J. Moon, A. A. Schafgans, S. Kasahara, T. Shibauchi, T. Terashima, Y. Matsuda, M. A. Tanatar, R. Prozorov, A. Thaler, P. C. Canfield, A. S. Sefat, D. Mandrus, and D. N. Basov, *Phys. Rev. Lett.* **109**, 027006 (2012).
- [39] P. Marsik, C. N. Wang, M. Rossle, M. Yazdi-Rizi, R. Schuster, K. W. Kim, A. Dubroka, D. Munzar, T. Wolf, X. H. Chen, and C. Bernhard, *Phys. Rev. B* **88**, 180508(R) (2013).
- [40] Y. M. Dai, A. Akrap, S. L. Bud'ko, P. C. Canfield, and C. C. Homes, *Phys. Rev. B* **94**, 195142 (2016).
- [41] G. E. Smith, L. C. Hebel, and J. Buchsbaum, *Phys. Rev.* **129**, 154 (1962).
- [42] J. Levallois, P. Chudziński, J. N. Hancock, A. B. Kuzmenko, and D. van der Marel, *Phys. Rev. B* **89**, 155123 (2014).
- [43] K. Momma and F. Izumi, *J. Appl. Cryst.* **44**, 1272 (2011).